HST Photometry of Dense Globular Cluster Fields: the Advantages of Deconvolution*

R. F. Butler

Dept. of Mathematics & Statistics, University of Edinburgh, UK

Abstract: It is shown that in very crowded fields, such as the cores of globular clusters, aperture photometry of subsampled-deconvolved HST/WFPC2 images gives statistically better results than any of the following *DAOPHOT-II* reductions of the original data: aperture photometry, profile-fitting photometry, and the hybrid method of aperture photometry on neighbour-subtracted images. Furthermore, the deconvolved images also provide the basis for improved star detection, using otherwise conventional means. These conclusions are developed and illustrated using both real HST/WFPC2 data of the Milky Way bulge globular cluster NGC 6293 in the F555W and F814W bands, and realistic simulations of a globular cluster observed under similar circumstances. The results are a consequence of exploiting the nature of the HST/WFPC2 point-spread function (PSF): undersampled, spatially varying and with high-frequency structure in the wings, but determinable to high accuracy by subsampled spatially-varying modelling of first-guess Tiny Tim grids followed by empirical improvements.

1 Introduction

The nature of the HST/WFPC2 point-spread function (PSF) is such that is is (1) undersampled by factors of 2 to 4 (Biretta et al. 1996); (2) spatially varying over the field of view (FOV) due to field-dependent aberrations etc.; and (3) characterised by considerable high-frequency structure in the "wings" ($r > (1 \rightarrow 2)\times$FWHM).

There are several problems which result from this. Firstly, residuals from determining & fitting the PSF to the image appear much larger than with well-sampled images. They make it difficult to cleanly subtract stars which are "neighbours" to the PSF stars; thus adding noise to empirical PSFs. Around bright stars they are similar in appearance to faint stars, thus causing errors in star detection (either missed detections of real objects, or false detections of "starlike" artefacts). Secondly, space-based telescopes preserve considerable high-frequency structure in the PSF wings; thus some wing features of bright stars can also mimic faint stars. Thirdly, undersampling reduces the statistical accuracy of the fit.

Furthermore, the conventional approach for crowded-field photometry (PSF-fitting) must perform a simultaneous least-squares fit to all of the detected stars; thus measurement errors are induced unless all the stars which should be grouped together are reduced together. Avoiding this makes the process very resource-hungry and computationally intensive - and hence slow.

*Based in part upon Hubble Space Telescope (HST) data obtained from the archive of Space Telescope - European Coordinating Facility (ST-ECF, ESO, Garching, Germany)

2 Method and Goals

To overcome the problems outlined above when performing photometry in the dense core fields of globular clusters, a new approach was developed. The HST/WFPC2 images were preprocessed using the Maximum Entropy Method (MEM) for image deconvolution (Narayan & Nityananda 1986, Skilling & Bryan 1984). The *STSDAS* implementation of MEM can handle expected noise sources (ie. Poisson photon-counting noise plus Gaussian read-out noise, suitable for the WFPC2), and it permits subsampling (subpixelisation) of the PSF and output image (suitable for the undersampled HST/WFPC2 images). However, the PSF must be spatially-invariant, so deconvolution was performed on a 6×6 grid of highly overlapping 256×256 pixel subimages, each with its own PSF appropriate to that position on the chip. The deconvolved subimages were then reassembled into a subsampled whole, upon which the star detection and photometry steps were performed. To reduce the number of potential false detections of "stars" which were actually deconvolution artefacts around the brighter stars, MEM-deconvolved images in two bands (F555W and F814W) were coadded with a moderate rejection threshold for statistically deviant positive features. This was very effective at eliminating artefacts because real stars hold steady in position, whereas deconvolution artefacts from slight PSF mismatches displace radially in the wings of stars according to the wavelength of light observed. Coadding also provided slightly greater depth - averaging out the background noise fluctuations while reinforcing the signal from faint stars.

The goals of this approach were as follows. Firstly, one would expect improved star detection on the subsampled MEM-deconvolved images, because the actual complex HST PSF shape (recall that it is undersampled, spatially varying, and has high-frequency structure in the "wings") is used in the star detection process via MEM, which effectively "Gaussianises" the PSF, doubles the sampling, and better separates the stars from each other. There was also the possibility of actually improving the photometric accuracy over conventional methods: so this work also sought to investigate whether aperture photometry on the subsampled MEM-deconvolved images was superior to all of the following conventional reductions of the original data: aperture photometry, profile-fitting photometry, and the hybrid method (eg. Yanny et al. 1994) of aperture photometry on neighbour-subtracted images.

Critical to the success of this approach was obtaining a first PSF model which is subsampled, noiseless, quadratically variable in a spatial sense, and a good match to the real PSF without being dependent on any analysis of the real data at this stage. For this model, the "stars" were a uniformly distributed 6×6 grid of normal-sampled *Tiny Tim* (Krist & Hook, 1996) synthetic PSFs for each WFPC2 chip & filter combination. A "moffat25" analytic function and six look-up tables were used to compute the 2× subsampled model PSF in *DAOPHOT-II* (Stetson 1994). The model PSF was quadratically variable over the image, with terms proportional to 1, x, y, x^2, xy, y^2. Residuals from fitting this model against the *Tiny Tim* F814W & F555W input grids are $\leq$2% in the core pixels of each "star" but can be $\approx$50% further out in the wings ($r>\approx$10 pixels).

All real HST data departs in some ways from the idealised models predicted by *Tiny Tim*, so a second PSF Model was needed to empirically improve upon the first. After star detection (as described above) on the coadded MEM images with *DAOPHOT-II/DAOFIND*, and a first *DAOPHOT-II/ALLSTAR* PSF-fit of the original images, a new subsampled, quadratically variable model was empirically computed from $\sim$90 - 100 bright stars. This second, refined PSF was then used to repeat the MEM deconvolution and PSF-fitting steps.

2.1 Simulations: the Cluster Model

In addition to testing these procedures on the real HST/WFPC2 data of the Milky Way bulge globular cluster NGC 6293 in the F555W and F814W bands, other cluster images were simulated in order to quantify the photometric and astrometric performance of the technique.

For the simulated images, there were 19957 input stars in total, of which 17175 were centred within the FOV. The remainder were centred outside the FOV, up to a further distance equal to the radius of the PSF. The spatial distribution of stars was based upon the NGC 6293 fitted surface brightness profile of Trager et al. (1995) but taking a steeper form in the core. The isochrone/luminosity functions of Bertelli et al. (1994) were used for the magnitude/colour distribution of the stars; the {Z=0.0040, Y=0.24, Age=14 Gyr} model was selected here. The apparent distance modulus (=16.0) for NGC 6293 of Janes & Heasley (1991), and the HST zeropoints & HST STMAG→Johnson/Cousins photometric system calibrations of Holtzman et al. (1995) and Whitmore (1995) were used to determine the intensity scale. The same net gain, readnoise, exposure time, saturation level, and mean background as the NGC 6293 images were all adopted to match the instrumental and observation conditions. The input PSF was constructed as described above, ie. as a *DAOPHOT-II* model of a *Tiny Tim* grid, but with 0".015 rms pointing-jitter, to add a coarse-lock degree of PSF blurring noise. Finally, the stars were simulated using *DAOPHOT-II/ADDSTAR* (not the conventional *IRAF/MKOBJECTS*) - because it permits the use of the 2×-subsampled, spatially varying form of the PSF.

3 Results: Photometry & Astrometry of the Simulated Images

Figure 1 shows the CMDs resulting from each of six different reduction procedures applied to the simulated images. Table 1 gives the corresponding statistics for the ΔC (= Colour(Out) - Colour(In)) values. The "bright" sample is defined as stars with $Vin < 20$; the "faint" sample as stars with $Vin \geq 20$. Small σ(ΔC) indicates low scatter in the CMD; non-zero Median(ΔC) indicates an offset (which can be calibrated out) in the colour index. Figure 2 illustrates these ΔC distributions graphically.

Figure 3 shows an astrometric analysis of the reduction of the simulated images. Note that in Fig. 3(a), 78% of all the detected stars have astrometric accuracies better than 0.1 pixels (bins 1-2), while there is a power law decline due to noise (fit overplotted) from bin 3 onwards. In particular, note the clear sub-pixel pattern in Fig. 3(d): this indicates that systematic errors are induced at a level ≤0.1 pixel.

Reduction Type	Sample Type	Number of Stars	σ(ΔC)	Median(ΔC)
(a) 1st PSF-fit	bright	943	0.091	-0.056
(b) 2nd PSF-fit	bright	935	0.043	0.009
(c) Aperture phot	bright	950	0.067	-0.488
(d) Hybrid, 2nd PSF	bright	931	0.031	-0.488
(e) MEM, 1st PSF	bright	951	0.056	-0.344
(f) MEM, 2nd PSF	bright	937	0.035	-0.366
(a) 1st PSF-fit	faint	12400	0.168	-0.029
(b) 2nd PSF-fit	faint	12406	0.121	0.018
(c) Aperture phot	faint	11976	0.148	-0.471
(d) Hybrid, 2nd PSF	faint	12303	0.106	-0.477
(e) MEM, 1st PSF	faint	12494	0.083	-0.320
(f) MEM, 2nd PSF	faint	12435	0.095	-0.363

Table 1: Statistics for the ΔC (= Colour(Out) - Colour(In)) values.

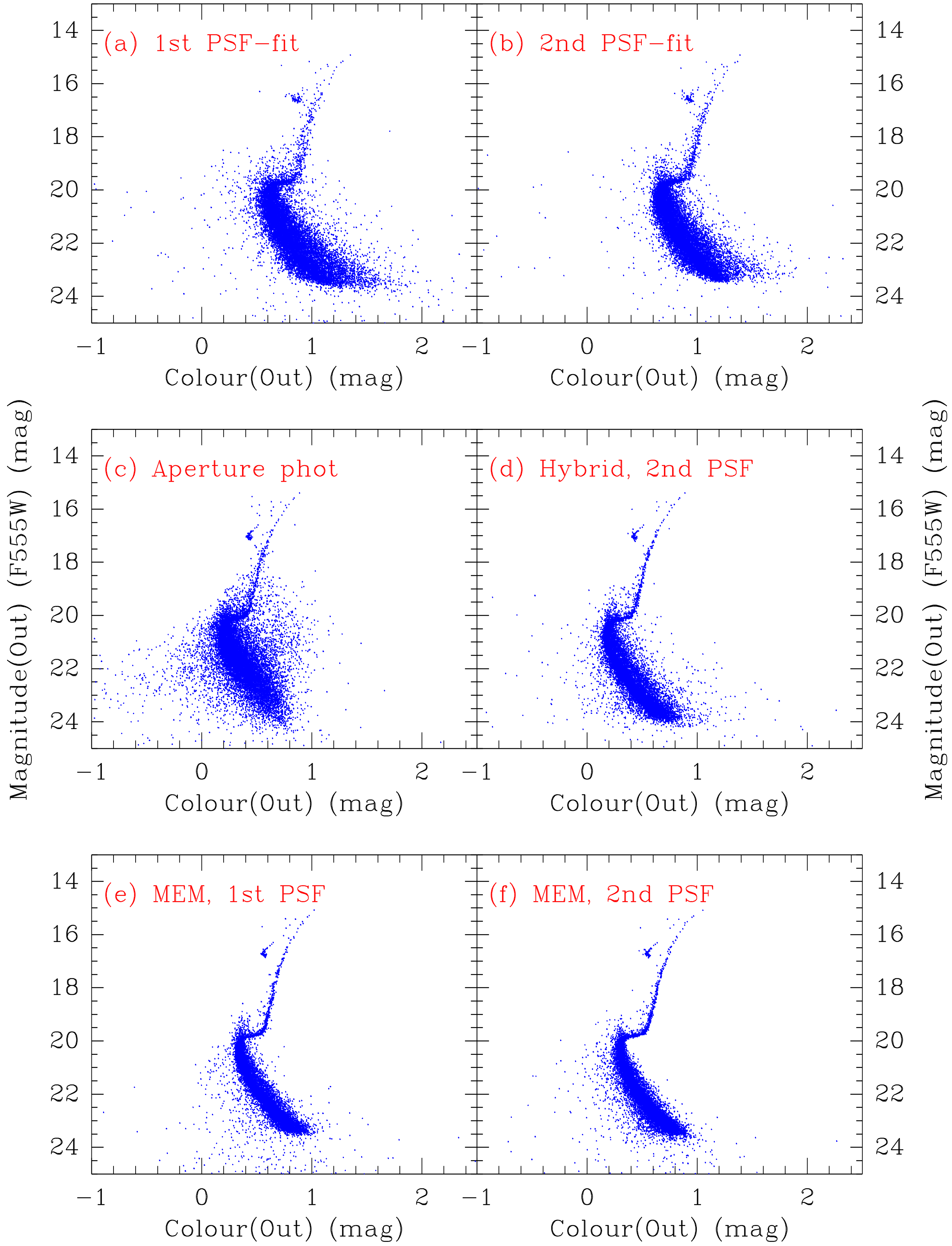

Figure 1: CMDs resulting from the various reduction techniques, for all stars in the simulated WFPC2/PC1 images.

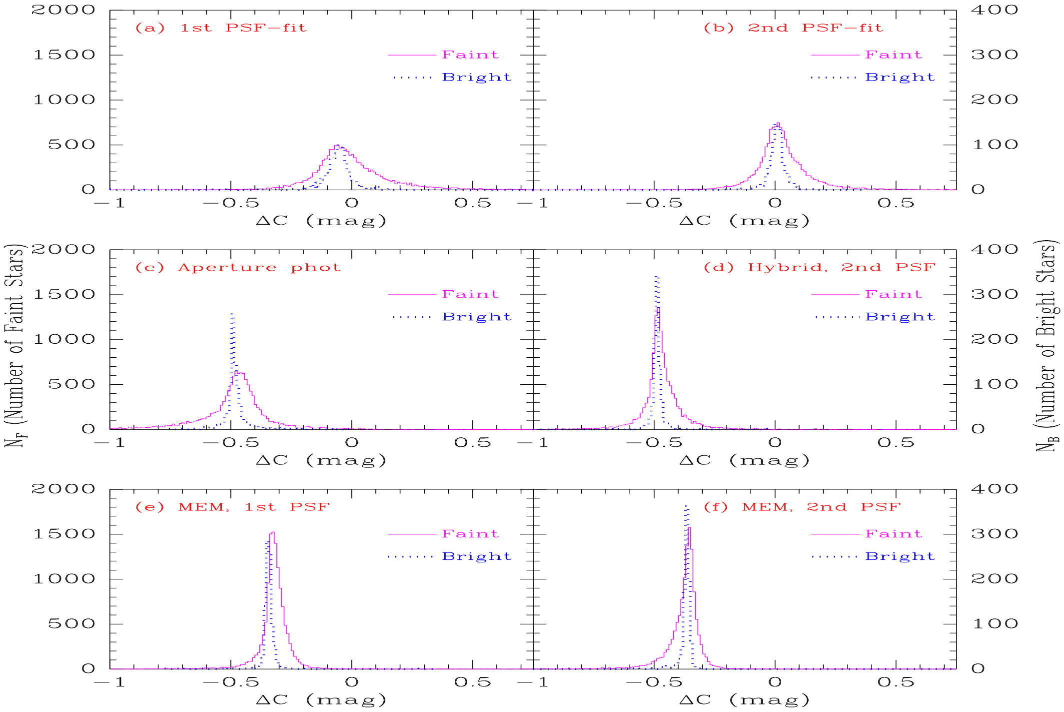

Figure 2: Histograms of ΔC (= Colour(Out) - Colour(In)), corresponding to the CMDs for all stars in Fig. 1 and the samples defined in Table 1.

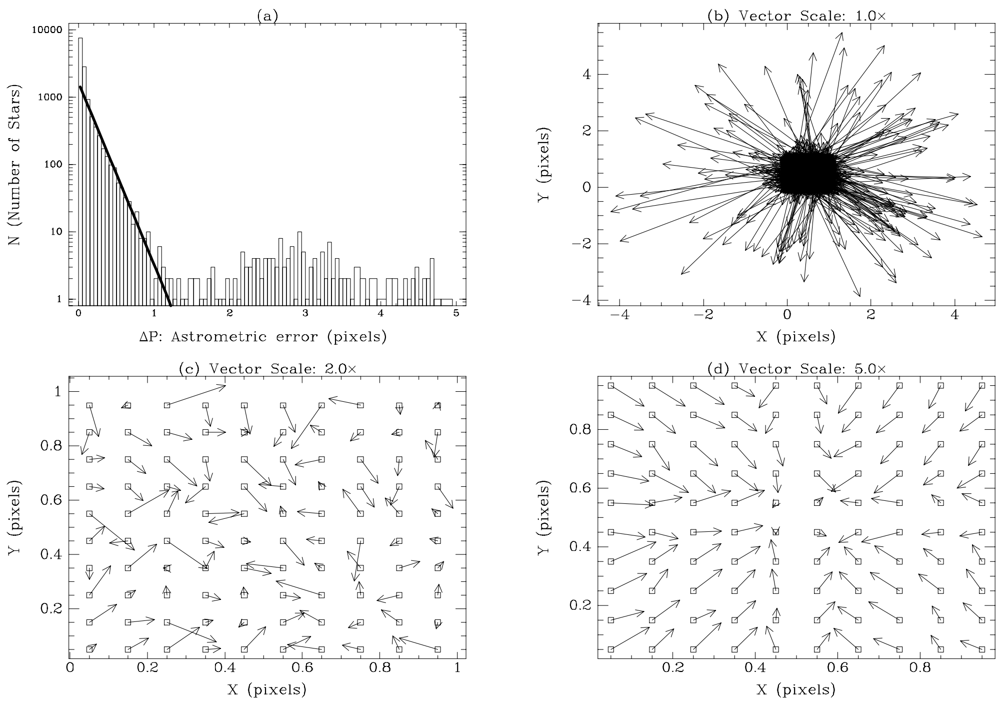

Figure 3: Astrometric analysis of the reduction of the simulated images. (a): Histogram of the ΔP $(= \sqrt{(\Delta x)^2 + (\Delta y)^2})$ astrometric errors for all detected objects. 1 bin = 0.05 pixel. (b): ΔP vectors with respect to the center of the pixel containing each star's peak (following Lindler et al. 1994). (c): As (b) but with vectors rebinned into 100 sub-pixel cells (on a 10×10 grid); vector magnification is 2.0× for clarity. (d): As (c) but only for stars with $\Delta P \leq 0.1$ pixel; vector magnification is 5.0×.

4 Conclusions

Despite some limitations in the models for the simulated images, we can still compare the *relative performance* of the reduction techniques. Star detection rates were indeed improved with the subsampled MEM-deconvolved images: for the same relative thresholds on the simulated images, 9446 stars were found with conventional methods, but 13528 stars with MEM-preprocessing, from an input total of 17175 stars. The improvement in the photometric accuracy was more moderate. Table 1 and Fig. 2 show that aperture photometry on the subsampled MEM-deconvolved images was on a par with the hybrid method for bright objects, and somewhat better for faint objects, thus statistically better overall. Although not shown here, similar gains in star detection and photometric quality were apparent in the case of NGC 6293. The astrometric accuracy of the new technique is limited by a systematic sub-pixel astrometric error at the $\leq$0.1 pixel level, induced by the MEM deconvolution (see Fig. 3(d)). This is fine for the purpose of crowded-field photometry, but precludes the use of this technique for high-precision astrometry. Selection by the "distance to nearest neighbour" parameter, ΔZ, can be used to produce a remarkably tight CMD, for analyses where individual stars are of little consequence but the aggregate structure is critical - eg. isochrone fitting, luminosity & mass functions.

One would not expect that the particular deconvolution algorithm used matters, providing that it can handle the noise sources and produce subsampled output with a subsampled PSF. Apart from MEM, there may be gains - particularly in the environs of strong sources - from newer algorithms such as that of Magain et al. (1998), which handles sampling correctly.

Acknowledgements

This research was supported by the TMR programme of the European Commission (contract ERBFMBICT972185). I am also grateful to my Edinburgh host, Prof. Douglas Heggie, Dr. Andy Shearer & Dr. Aaron Golden (NUI Galway, Ireland) and Dr. Alan Penny (RAL, UK) for their advice and encouragement.

References

Bertelli G., Bressan A., Chiosi C., Fagotto F., Nasi E., 1994, A&AS 106, 275

Biretta J. A., et al., 1996, WFPC2 Instrument Handbook, Version 4.0 (Baltimore: STScI)

Holtzman J., et al., 1995, PASP 107, 1065

Janes K. A., Heasley J. N., 1991, AJ 101, 2097

Krist J., Hook R., 1996, Tiny Tim User's Manual, Version 4.2 (Baltimore: STScI)

Lindler D., Heap S., Holbrook J., Malumuth E., Norman D., Vener-Saavedra P. C., 1994, in "The Restoration of HST Images and Spectra II" (Baltimore: STScI)

Magain P., Courbin F., Sohy S., 1998, ApJ 494, 472

Narayan R., Nityananda R., 1986, Ann.Rev.A&A 24, 127

Skilling J., Bryan R. K., 1984, MNRAS 211, 111

Stetson P. B., 1994, PASP 106, 250

Trager S.C., King I.R., Djorgovski S., 1995, AJ 109, 218

Whitmore B., 1995, in "Calibrating Hubble Space Telescope. Post Servicing Mission", (Baltimore: STScI)

Yanny B., Guhathakurta P., Schneider D., Bahcall J., 1994, ApJ 435, L59